1    **A D- and ^{15}N-rich micrometer-sized aggregate of organic matter in a xenolithic clast from**

2    **the Zag ordinary chondrite**

3

4    Yoko Kebukawa[1]*, Motoo Ito[2], Michael E. Zolensky[3], Zia Rahman[4], Hiroki Suga[5], Aiko

5    Nakato[6], Queenie H. S. Chan[3][†], Marc Fries[3], Yasuo Takeichi[7], Yoshio Takahashi[8], Kazuhiko

6    Mase[7], and Kensei Kobayashi[1]

7

8    *Corresponding author: kebukawa@ynu.ac.jp

9

10    [1]Faculty of Engineering, Yokohama National University, 79-5 Tokiwadai, Hodogaya-ku,

11    Yokohama 240-8501, Japan

12    [2]Kochi Institute for Core Sample Research, JAMSTEC, B200 Monobe, Nankoku, Kochi 783-

13    8502, Japan

14    [3]ARES, NASA Johnson Space Center, 2101 NASA Parkway, Houston, TX 77058, USA

15    [4]Jacobs, NASA Johnson Space Center, Houston, TX 77058, USA

16    [5]Department of Earth and Planetary Systems Science, Hiroshima University, Kagamiyama,

17    Higashi-Hiroshima, Hiroshima 739-8526, Japan

18    [6] Graduate School of Science, Kyoto University, Kitashirakawa Oiwake-cho, Sakyo-ku, Kyoto

19    606-8502, Japan

20    [7]Institute of Materials Structure Science, High-Energy Accelerator Research Organization (KEK),

21    1-1 Oho, Tsukuba, Ibaraki 305-0801, Japan

22    [8]Department of Earth and Planetary Science, The University of Tokyo, Hongo, Bunkyo-ku,

23    Tokyo 113-0033, Japan

24    [†]Current address: Department of Physical Sciences, The Open University, Walton Hall, Milton

25    Keynes, MK7 6AA, UK

26

27

28    **Summary**

29        The nature and origin of extraterrestrial organic matter are still under debate despite the

30    significant progress in the analyses and experimental approaches in this field over the last five

31    decades. Xenolithic clasts are often found in a wide variety of meteorite groups[1-8], some of

32    which contain exotic organic matter (OM). The Zag meteorite is a thermally-metamorphosed H

33    ordinary chondrite. It contains a primitive xenolithic clast that has been proposed to have

34    originated from Ceres[9-11], which was accreted to the Zag host asteroid after metamorphism. The

35    cm-sized clast contains abundant large carbon-rich (mostly organic) grains or aggregates up to

36    20 μm[10-12]. Such large OM grains are unique among astromaterials with respect to the size. Here

37    we report organic and isotope analyses of a large (~10 μm) aggregate of solid OM in the Zag

38    clast. The X-ray micro-spectroscopic technique revealed that the OM has $sp^2$ bonded carbon with

39    no other functional groups nor graphitic feature (1s-σ* exciton), and thus it is distinguished from

40    most of the OM in carbonaceous meteorites. The apparent absence of functional groups in the

41    OM suggests that it is composed of hydrocarbon networks with less heteroatoms, and therefore

42    the OM aggregate is similar to hydrogenated amorphous carbon (HAC)[13-18]. The OM aggregate

43    has high D/H and $^{15}N/^{14}N$ ratios, suggesting that it originated in a very cold environment such as

44    the interstellar medium or outer region of the solar nebula, while the OM is embedded in

45    carbonate-bearing matrix resulting from aqueous activities. Thus the high D/H ratio must have

46    survived the extensive late-stage aqueous processing. It is not in the case for OM in

47    carbonaceous chondrites of which the D/H ratio was reduced by the alteration via the D-H

48    exchange of water[19]. It indicates that both the OM precursors and the water had high D/H ratios,

49    similar to the water in Enceladus[20]. Our results support the idea that the clast originated from

50    Ceres, or at least, a hydrovolcanically active body similar to Ceres, and further imply that Ceres

51    originally formed in the outer Solar System and migrated to the main belt asteroid region[21] as

52    suggested by the "Grand tack" scenario[22].

53

54  _____

55         Xenolithic clasts are present in a wide variety of meteorite groups[1-8]. These clasts have

56    been protected in host meteorites that are typically more metamorphosed and thus are physically

57    strengthened by thermal annealing via heating processes occurring prior to the incorporation of

58    the clasts. Hence, such clasts can contain primitive and fragile materials that would not have

59    survived parent body alteration processes and atmospheric entry. The Zag meteorite is a H3-6

60    chondrite which fell in Morocco on August 1998, and is known to contain xenolithic, fluid

61    inclusion-bearing halite crystals and a centimeter-sized carbonaceous chondrite-like clast[1]. These

62    clasts and halite crystals in the Zag meteorite have been proposed to be materials from dwarf

63    planet 1/Ceres in light of their mineralogy and the orbital dynamics of a possible parent body[9,11].

64    The Zag clast consists of saponite, serpentine, Ca-Fe-Mg carbonates, Fe-Ni sulfides, magnetite,

65    halite, minor olivine and pyroxene, as well as abundant large OM grains or aggregates up to 20

66    μm (Fig. 1), all consistent with formation on a large, aqueously active, carbonaceous body, e.g.,

67    Ceres[10,11,23]. Ceres' orbit crosses that of the proposed H chondrite parent body, asteroid

68    6/Hebe[9,24]. The current mean infall velocity of material transferred from Ceres to Hebe is

69    approximately 1.20 to 1.38 km/s, although this transfer velocity could have been lower in the

70    past[9]. This infall velocity is generally relatively low for transfer of material between inner Solar

71    System bodies and thus survival of fragile material would be possible.

72    We analyzed the molecular structure and isotope chemistry of a focused ion beam (FIB)

73    ultra-thin section obtained from an OM aggregate using scanning transmission X-ray microscopy

74    (STXM) and nanoscale secondary ion mass spectrometry (NanoSIMS).

75
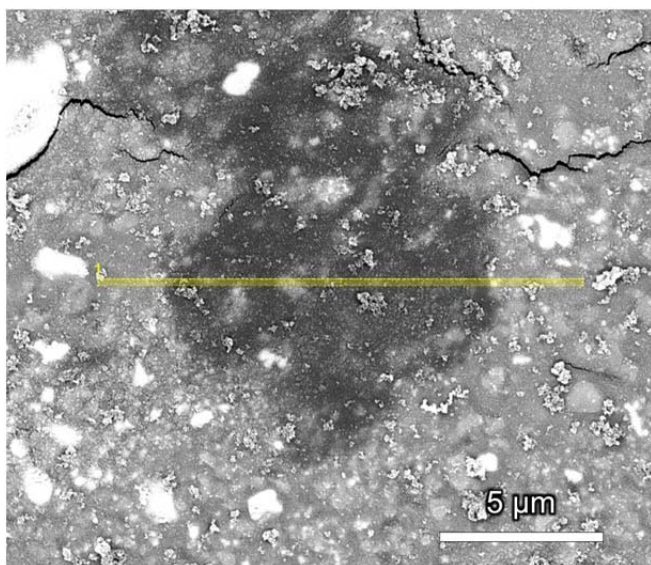
76



77    **Fig. 1: Backscattered electron (BSE) image of a polished thin section of the organic**

78    **aggregate (dark) in the carbonaceous clast in the Zag meteorite.** FIB section was subsample

79    from yellow region.

80

81    The FIB section obtained from the OM aggregate (Fig. 1) showed a large carbon-

82    dominated area over 10 μm in width that corresponded to the OM aggregate (**Fig. 2**). A carbon

83    X-ray absorption near edge structure (C-XANES) spectrum of the OM aggregate showed a peak

84    at 284.8 eV that is assigned to $sp^2$ (aromatic) carbon (**Fig. 2**b,c in red). The surrounding matrix

85    area showed a peak at 290.3 eV that is assigned to carbonates ($CO_3$) with some organic features

86    at 284.8 eV, 286.3 eV (assigned to ketone [C=O]) and 288.5 eV (assigned to carboxyl/ester

87    [(C=O)O]) (**Fig. 2**b,c in green). The C-XANES spectrum of the OM aggregate does not show

88    other peaks that are characteristic of insoluble organic matter (IOM) in primitive chondrites (e.g.,

89    C=O and (C=O)O indicating primitive OM in Murchison meteorite)[25], nor that in the thermally-

90    metamorphosed meteorites (e.g., 1s-σ* exciton at 291.7 eV indicating graphene structures in the

91    Allende meteorite)[26]. The C-XANES of the OM aggregate most resembles $sp^2$-rich hydrogenated

92    amorphous carbon (HAC, also written as a-C:H) like material[13-18]. No detectable nitrogen

93    features were observed in N-XANES spectra of the OM aggregate, probably due to low

94    concentration of nitrogen, while matrix showed a small peak at 401.0 eV that is tentatively

95    assigned to amine or NH containing heterocycles[27,28] (**Fig. 2**d). The 401.0 eV peak could be

96    atmospheric $N_2$ which was either trapped in the inorganic phase or generated during X-ray

97    exposure[28], but high $\delta^{15}N$ (shown below) in the matrix area indicate the presence of indigenous

98    nitrogen compounds.

99        **Fig. 3** shows high spatial resolution secondary ion mass spectrometry (NanoSIMS)

100   isotope $\delta D$, $\delta^{15}N$ and $^{12}C^{14}N/^{16}O$ images of the FIB section containing the OM aggregate (same

101   section shown in **Fig. 2**). Hydrogen, nitrogen and carbon isotopic and elemental ratios of the OM

102   aggregate and surrounding matrix are summarized in **Table 1**. The OM aggregate had a large $\delta D$

103   and $\delta^{15}N$ anomaly; $\delta D = 2,370 \pm 74$ ‰ and $\delta^{15}N = 696 \pm 100$ ‰ on average. The $\delta^{13}C$ value was

104   $-43 \pm 20$ ‰ that was broadly consistent with the values of IOM from CR chondrites and the

105   Bells meteorite (an unusual CM2 chondrite)[19] within analytical error. Two isotopic hot spots

106   were observed; one is D- and $^{15}N$-rich ($\delta D = 4,200 \pm 550$ ‰ and $\delta^{15}N = 3,413 \pm 1,070$ ‰), and

107   the other is D-rich ($\delta D = 4,500 \pm 900$ ‰) and less $^{15}N$-rich ($724 \pm 780$ ‰) (Fig. 3e,f). These

108   enrichments of the heavy isotopes suggest that the OM or its precursors formed by low-

109   temperature chemistry in molecular clouds or the outer protosolar disk[29]. The origin of the

110   isotope heterogeneities (hot spots) in the OM aggregate in the Zag clast is puzzling since no

111   molecular heterogeneity was observed between the hot spots and the average OM area (**Fig. 2**c).

112         N-XANES spectra and NanoSIMS $^{12}C^{14}N/^{16}O$ images of the Zag clast FIB section

113   showed a relatively high concentration of nitrogen in the matrix region. A rough estimation by

114   NanoSIMS for N/C elemental ratio of matrix was $0.036 \pm 0.006$ while N/C ratio of OM

115   aggregate was $0.022 \pm 0.003$. The majority of carbon in the matrix comes from carbonates,

116   therefore the $N/C_{OM}$ ratio of the matrix would have been higher.

117
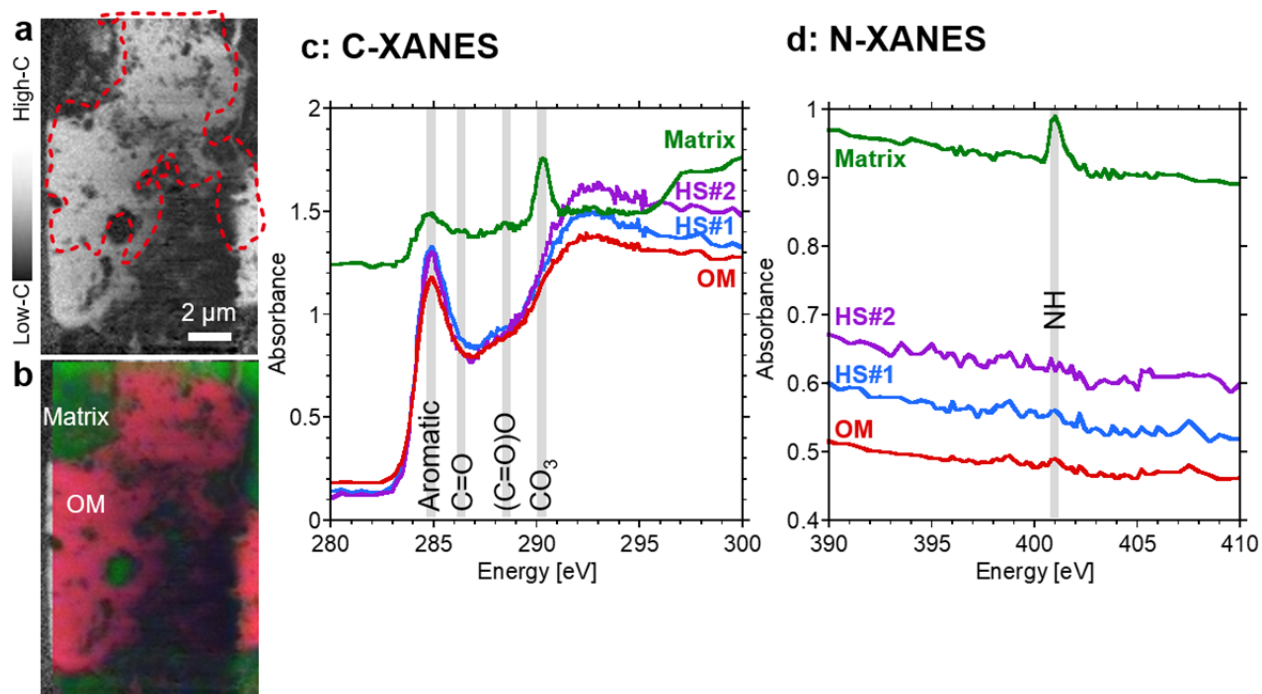


118

119   **Fig. 2: Scanning transmission X-ray microscopy (STXM) analyses of a focused ion**

120   **beam (FIB) section containing the organic matter (OM) aggregate in the Zag clast.** (a)

121   Carbon-map indicates the section is dominated by carbon. The location of the δD image (**Fig. 3**)

122   is indicated by red dots. (b) Composition map derived from C-XANES of OM (red) and matrix

123   (green). (c) Carbon X-ray absorption near-edge structure (C-XANES) of OM aggregate revealed

124   that it is hydrogenated amorphous carbon (HAC)-like material dominated by $sp^2$ carbon (284.8

eV) while the surrounding matrix is mainly carbonates (290.3 eV) with some OM at 286.3 eV that is assigned to ketone (C=O) and 288.5 eV that is assigned to carboxyl/ester [(C=O)O]. (d) The OM aggregate does not show detectable N-XANES features while matrix shows a peak at 401.0 eV which is assigned to amine or NH in heterocycles. The C- and N-XANES obtained from isotope hot spots (HS, see **Fig. 3**) are also shown.
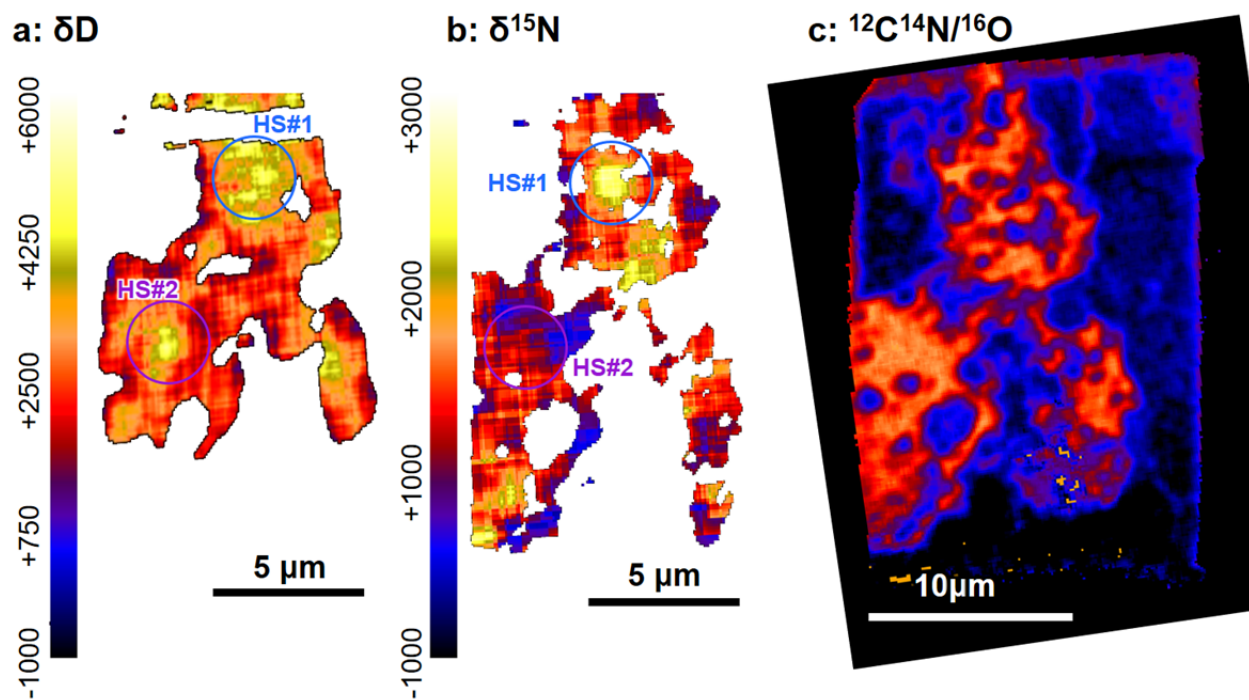


**Fig. 3: NanoSIMS isotope images of the FIB section containing the organic matter (OM) aggregate in the Zag clast (same section with Fig. 2).** (a) $\delta$D image (the location is indicated in red dots in **Fig. 2**a), (b) $\delta^{15}$N image and (c) $^{12}C^{14}N/^{16}O$ ratio image. Isotopic hot spots are indicated by circles.

**Table 1: Hydrogen, nitrogen and carbon isotopic and elemental ratios of organic**

**matter (OM) aggregate and matrix of the Zag clast measured by NanoSIMS.**

| | δD ‰ | δ15N ‰ | δ13C ‰ | H/C | N/C | O/C | O/C [a] |
|---|---|---|---|---|---|---|---|
| OM aggregate | 2,370±74 | 696±100 | −43±20 | 0.60±0.03 | 0.022±0.003 | 0.15±0.02 | ~0.06-0.07 |
| Hot spot #1 | 4,200±550 | 3,413±1,070 | | 0.41±0.02 | 0.032±0.006 | 0.16±0.02 | |
| Hot spot #2 | 4,500±900 | 724±780 | | | | | |
| Matrix | − | 301±98 | 10±41 | | 0.036±0.001 | | ~1.4-1.6 |

[a] Estimated by C,N,O *K*-edge X-ray absorption spectra.

The large, micrometer-sized OM grains/aggregates are abundant in the Zag clast but are rare in other meteorites - a very few are known in CR chondrites[30,31]. The OM aggregate in the Zag clast studied here is somewhat similar to ultracarbonaceous Antarctic micrometeorites (UCAMM) that are considered as cometary materials[32], with respect to the size and the high concentrations of heavy isotopes (D and ^{15}N). However, C- and N-XANES analyses of UCAMM indicated the presence of O- and N-bearing functional groups, e.g., C=O, (C=O)O, C=N, and NHx(C=O)[33,34], that is not the case for the OM aggregate in the Zag clast. Cometary OM (CHON particles from comet Halley and returned samples from comet 81P/Wild 2) has higher H, N and O contents, compared to the OM aggregates[35,36]. The C-XANES spectra of comet 81P/Wild2 particles, as well as anhydrous and hydrated chondritic interplanetary dust particles and chondritic micrometeorites (some of which probably originated from comets) also show O-bearing functional groups (e.g., C=O at ~286.5 eV, (C=O)O at ~288.5 eV)[35,37-39].

The C-XANES spectrum of the OM aggregate does not resemble IOM in primitive CI/CM/CR chondrites that shows C=O at ~286.5 eV, (C=O)O at ~288.5 eV and sometime aliphatic carbon at ~287.5 eV[25]. Even the C-XANES spectra of the IOM from thermally-

157 metamorphosed chondrites (e.g., CV and CO chondrites and ordinary chondrites) have a 288.5

158 eV peak, in addition to 1s-σ* exciton at 291.7 eV indicating graphene structures[26], this is not the

159 case for the OM aggregate. A rough estimation for the O/C elemental ratio of the OM aggregate

160 from C,N,O X-ray absorption spectra is 0.06 to 0.07 (the method is reported elsewhere[35]), that is

161 lower than IOM extracted from CV, CO and ordinary chondrites[19]. The O/C ratio obtained by

162 NanoSIMS was 0.15, which can be attributed to uncertainty of O/C ratio obtained by

163 NanoSIMS[40].

164       C-XANES spectra of "aromatic" nanoglobules in chondrites reported by De Gregorio et

165 al.[41] are similar to the OM aggregate in the Zag clast. In their study, some aromatic nanoglobules

166 tend to have higher $\delta^{15}N$ values than IOM-like nanoglobules, although the correlation between

167 molecular structure and $\delta^{15}N$ was rather ambiguous[41]. The OM aggregate has isotopic

168 heterogeneities without molecular structure heterogeneities, and it indicates that the OM

169 aggregate consists of materials with different origins but which subsequently experienced similar

170 chemical evolution pathways. Note that we also found a globular OM grain in the Zag clast

171 (Extended Data Figure 1) but larger (~5 μm) than typical nanoglobules (<1 μm).

172       The high D/H and $^{15}N/^{14}N$ ratios suggest that the OM aggregate originated in a very cold

173 environment such as the interstellar medium or the outer region of the solar nebula. The OM

174 aggregate is in close proximity to the aqueously altered matrix, which indicates that the OM

175 aggregate was processed by the same aqueous event as the surrounding matrix. The low

176 temperature and extended period of the aqueous event could have reduced substituted functional

177 groups of the OM structure.

178       In the case of carbonaceous chondrites, significant decreases in D/H ratio of OM are

179 accompanied by aqueous alteration mostly due to D-H exchange with D-poor water, e.g., the δD

180    value of OM in the most aqueously altered CI chondrites is ~970-980 ‰ in contrast to the high

181    $\delta$D values of the least altered carbonaceous chondritic OM (up to ~3500 ‰)[19]. If this is the case

182    of the Zag clast, the D/H ratio of the OM is expected to be reduced during the heavy aqueous

183    alteration reflected in the mineralogy of the clast, i.e., CI chondrite like compositions[10,11].

184    Therefore, D-rich water is required to maintain the high D/H ratio ($\delta$D ~ 2400 ‰) in the OM

185    aggregate, such as the water in Enceladus which has a D/H ratio of 2.9 (+1.5/−0.7) × $10^{-4}$ ($\delta$D ~

186    1820 to 410 ‰)[20]. Water in halite, which has plausibly the same origin as water in the clast,

187    shows a large variation of $\delta$D, −400 to +1300 ‰, and it is attributed to the variation in degree of

188    water-rock interactions[42].

189         The surrounding matrix contains N-rich compounds possibly in the form of amine or

190    heterocycles. These N-bearing compounds would not share the same origin with the OM

191    aggregate since the $\delta^{15}$N value of the OM is ~700 ± 100 ‰ while the matrix is ~300 ± 100 ‰.

192    IOM in carbonaceous chondrites is known to release ammonia up to 10 µg/mg via hydrothermal

193    processing at 300–400 °C, but the $\delta^{15}$N of the released fractions are higher than the original

194    IOM[43]. In any case, N-rich compounds and carbonates in the matrix of the Zag clast is consistent

195    with recent observation of ammoniated phyllosilicates and carbonates in the regolith of

196    Ceres[21,23,44].

197         The recent discovery of ammoniated phyllosilicates on the surface of Ceres implies that

198    material from the outer Solar System was incorporated into Ceres, either during its formation at

199    great heliocentric distance or by incorporation of material transported into the main asteroid belt

200    [21]. This is consistent with the high D/H and $^{15}$N/$^{14}$N ratios of the OM aggregate as well as the

201    observed extensive parent body aqueous alteration involving D-rich water. Our results further

202    support the idea that Ceres originated in the outer region of the Solar System, then migrated

203     inward to the main belt region scattered by migrations of Jupiter and Saturn as required by the

204     "Grand Tack" scenario[21,22]. Ceres could have originated as a salty ocean world similar to

205     Enceladus[45] and was subsequently transported to the main belt region where the icy ocean

206     sublimated to leave behind salts, carbonates, clays and organic matter.

207

208

213

214

## Methods

### *Sample preparation using a focused ion beam (FIB)*

The OM aggregate was selected from a polished thin section of the xenolithic clast in the Zag meteorite using imaging from a JEOL 7600F field emission gun scanning electron microscope (FEG-SEM) at NASA/JSC. Approximately 100 nm-thick sections were subsampled from the OM aggregate in the Zag clast using a Quanta 3d FEG focused ion beam (FIB) instrument at NASA/JSC.

### *Scanning-Transmission X-ray Microscopy (STXM)*

Carbon, nitrogen and oxygen X-ray absorption near edge structure (C,N,O-XANES) micro-spectroscopy was performed using the scanning-transmission X-ray microscopes (STXM) at BL13A of the Photon Factory, High Energy Accelerator Research Organization (KEK)[46,47]. The carbon map was obtained by acquiring pairs of images below and on the carbon *K*-edge, at 280 and 292 eV, respectively, and taking the $-\ln(I_{292}/I_{280})$ for each pixel. The C-XANES spectra were acquired with the energy step sizes ($\Delta E$) of 0.1 eV in 283–295.5 eV region, 0.5 eV in 280–283 eV and 295.5–301.0 eV regions, and 1 eV in 301–310 eV region. For N-XANES, $\Delta E$ was 0.2 eV in 395–406 eV region, 0.5 eV in 385–395 eV and 406–410 eV regions, and 2 eV in 410–430 eV region. For O-XANES, $\Delta E$ was 0.2 eV in 530–540 eV region, 1 eV in 520–530 eV and 540–560 eV regions, and 2 eV in 560–580 eV region. The acquisition time per energy step was 5 to 10 ms.

### *NanoSIMS ion microprobe*

237    H, C and N isotope imaging measurements of the Zag clast FIB section were carried out

238    with the JAMSTEC NanoSIMS 50L. Detailed measurement conditions are described

239    elsewhere[48,49]. Briefly, a focused $Cs^+$ primary ion beam of 0.8 to 4 pA was rastered over 25 µm x

240    25 µm areas on the sample and a standard material (1-hydroxybenzotriazole hydrate;

241    $C_6H_5N_3O \cdot xH_2O$, calculated as x=1). The spatial resolution was estimated to be ~100 nm for C

242    and N isotope images, and ~200 nm for H isotope image. Each run repeatedly scanned (10 to 20

243    times) over the same area. Individual images consist of 256 x 256 pixels with acquisition time of

244    6,000 µs/pixel (393 sec/frame) for C and N isotope images, and of 5,000 µs/pixel (328

245    sec/frame) for H isotope image. Each measurement was started after stabilization of the

246    secondary ion intensities following a pre-sputtering procedure of approximately 1–3 min. The

247    sample was coated with a 10 nm Au thin film to mitigate electrostatic charge on the surface.

248    During the analysis, the mass peaks were centered automatically every 5 cycles.

249

250

251    **References**

252    1    Rubin, A. E., Zolensky, M. E. & Bodnar, R. J. The halite‐bearing Zag and Monahans
253         (1998) meteorite breccias: Shock metamorphism, thermal metamorphism and aqueous
254         alteration on the H‐chondrite parent body. *Meteoritics & Planetary Science* **37**, 125-141
255         (2002).
256    2    Brearley, A. J. Carbon-rich aggregates in type 3 ordinary chondrites: Characterization,
257         origins, and thermal history. *Geochimica et Cosmochimica Acta* **54**, 831-850,
258         doi:10.1016/0016-7037(90)90377-W (1990).
259    3    Buchanan, P., Zolensky, M. & Reid, A. Carbonaceous chondrite clasts in the howardites
260         Bholghati and EET87513. *Meteoritics* **28**, 659-669 (1993).
261    4    Zolensky, M. *et al.* Mineralogy, petrology and geochemistry of carbonaceous chondritic
262         clasts in the LEW 85300 polymict eucrite. *Meteoritics* **27**, 596-604 (1992).
263    5    Zolensky, M. E. Asteroidal Water Within Fluid Inclusion-Bearing Halite in an H5
264         Chondrite, Monahans (1998). *Science* **285**, 1377-1379,
265         doi:10.1126/science.285.5432.1377 (1999).

266    6    Zolensky, M. E., Weisberg, M. K., Buchanan, P. C. & Mittlefehldt, D. W. Mineralogy of
267        carbonaceous chondrite clasts in HED achondrites and the Moon. *Meteoritics &*
268        *Planetary Science* **31**, 518-537 (1996).

269    7    Nakashima, D., Nakamura, T. & Noguchi, T. Formation history of CI-like phyllosilicate-
270        rich clasts in the Tsukuba meteorite inferred from mineralogy and noble gas signatures.
271        *Earth and Planetary Science Letters* **212**, 321-336 (2003).

272    8    Brearley, A. J. CI chondrite-like clasts in the Nilpena polymict ureilite: Implications for
273        aqueous alteration processes in CI chondrites. *Geochimica et Cosmochimica Acta* **56**,
274        1373-1386 (1992).

275    9    Fries, M., Messenger, S., Steele, A. & Zolensky, M. Do We Already have Samples of
276        Ceres? H Chondrite Halites and the Ceres-Hebe Link. *76th Annual Meeting of the*
277        *Meteoritical Society*, Abstract #5266 (2013).

278   10    Zolensky, M. *et al.* The Mineralogy of Ceres*(* Or Something an Awful Lot Like It).
279        *78th Annual Meeting of the Meteoritical Society*, Abstract #5270 (2015).

280   11    Zolensky, M. E. *et al.* The search for and analysis of direct samples of early Solar System
281        aqueous fluids. *Philosophical Transactions of the Royal Society A: Mathematical,*
282        *Physical and Engineering Sciences* **375**, doi:10.1098/rsta.2015.0386 (2017).

283   12    Fries, M., Zolensky, M. & Steele, A. Mineral inclusions in Monahans and Zag halites:
284        Evidence of the originating body. *Meteoritics and Planetary Science Supplement* **74**
285        (2011).

286   13    Robertson, J. Hard amorphous (diamond-like) carbons. *Progress in Solid State Chemistry*
287        **21**, 199-333 (1991).

288   14    Ray, S. C. *et al.* Studies of ion irradiation effects in hydrogenated amorphous carbon thin
289        films by X-ray absorption and photoemission spectroscopy. *Thin Solid Films* **516**, 3374-
290        3377, doi:10.1016/j.tsf.2007.10.020 (2008).

291   15    Buijnsters, J. G. *et al.* Hydrogen quantification in hydrogenated amorphous carbon films
292        by infrared, Raman, and x-ray absorption near edge spectroscopies. *Journal of Applied*
293        *Physics* **105**, doi:10.1063/1.3103326 (2009).

294   16    Buijnsters, J. G., Gago, R., Redondo-Cubero, A. & Jimenez, I. Hydrogen stability in
295        hydrogenated amorphous carbon films with polymer-like and diamond-like structure.
296        *Journal of Applied Physics* **112**, doi:10.1063/1.4764001 (2012).

297   17    Tunmee, S. *et al.* Study of Synchrotron Radiation Near-Edge X-Ray Absorption Fine-
298        Structure of Amorphous Hydrogenated Carbon Films at Various Thicknesses. *Journal of*
299        *Nanomaterials*, doi:10.1155/2015/276790 (2015).

300   18    Jia, L. Y. *et al.* Effect of gas residence time on near-edge X-ray absorption fine structures
301        of hydrogenated amorphous carbon films grown by plasma-enhanced chemical vapor
302        deposition. *Japanese Journal of Applied Physics* **55**, doi:10.7567/jjap.55.040305 (2016).

303   19    Alexander, C. M. O. D., Fogel, M., Yabuta, H. & Cody, G. D. The origin and evolution
304        of chondrites recorded in the elemental and isotopic compositions of their
305        macromolecular organic matter. *Geochimica et Cosmochimica Acta* **71**, 4380-4403,
306        doi:10.1016/j.gca.2007.06.052 (2007).

307   20    Waite Jr, J. H. *et al.* Liquid water on Enceladus from observations of ammonia and 40Ar
308        in the plume. *Nature* **460**, 487-490,
309        doi:http://www.nature.com/nature/journal/v460/n7254/suppinfo/nature08153_S1.html
310        (2009).

311    21    De Sanctis, M. C. *et al.* Ammoniated phyllosilicates with a likely outer Solar System
312           origin on (1) Ceres. *Nature* **528**, 241-244, doi:10.1038/nature16172 (2015).

313    22    Walsh, K. J., Morbidelli, A., Raymond, S. N., O'Brien, D. P. & Mandell, A. M. A low
314           mass for Mars from Jupiter/'s early gas-driven migration. *Nature* **475**, 206-209 (2011).

315    23    McSween, H. Y. *et al.* Carbonaceous chondrites as analogs for the composition and
316           alteration of Ceres. *Meteoritics & Planetary Science* **in press**, doi:10.1111/maps.12947
317           (2017).

318    24    Gaffey, M. J. & Gilbert, S. L. Asteroid 6 Hebe: The probable parent body of the H‐type
319           ordinary chondrites and the IIE iron meteorites. *Meteoritics & Planetary Science* **33**,
320           1281-1295, doi:10.1111/j.1945-5100.1998.tb01312.x (1998).

321    25    Le Guillou, C., Bernard, S., Brearley, A. J. & Remusat, L. Evolution of organic matter in
322           Orgueil, Murchison and Renazzo during parent body aqueous alteration: In situ
323           investigations. *Geochimica et Cosmochimica Acta* **131**, 368-392,
324           doi:10.1016/j.gca.2013.11.020 (2014).

325    26    Cody, G. D. *et al.* Organic thermometry for chondritic parent bodies. *Earth and*
326           *Planetary Science Letters* **272**, 446-455, doi:10.1016/j.epsl.2008.05.008 (2008).

327    27    Newbury, D., Ishii, I. & Hitchcock, A. Inner shell electron-energy loss spectroscopy of
328           some heterocyclic molecules. *Canadian Journal of Chemistry* **64**, 1145-1155 (1986).

329    28    Leinweber, P. *et al.* Nitrogen K-edge XANES - an overview of reference compounds
330           used to identify `unknown' organic nitrogen in environmental samples. *Journal of*
331           *Synchrotron Radiation* **14**, 500-511, doi:doi:10.1107/S0909049507042513 (2007).

332    29    Yang, J. & Epstein, S. Interstellar organic-matter in meteorites. *Geochimica et*
333           *Cosmochimica Acta* **47**, 2199-2216, doi:10.1016/0016-7037(83)90043-1 (1983).

334    30    Peeters, Z., Changela, H., Stroud, R., Alexander, C. & Nittler, L. in *Lunar and Planetary*
335           *Science Conference.*

336    31    J. Leitner, C. V., P. Hoppe. A SEM AND NANOSIMS INVESTIGATION OF
337           ORGANIC AGGREGATES IN THE CR CHONDRITES MILLER RANGE 07525 AND
338           RENAZZO. *80th Annual Meeting of the Meteoritical Society 2017 (LPI Contrib. No.*
339           *1987)* (2017).

340    32    Duprat, J. *et al.* Extreme deuterium excesses in ultracarbonaceous micrometeorites from
341           central Antarctic snow. *Science* **328**, 742-745, doi:10.1126/science.1184832 (2010).

342    33    Engrand, C. *et al.* in *Lunar and Planetary Science Conference.* 1902.

343    34    Yabuta, H. *et al.* Formation of an ultracarbonaceous Antarctic micrometeorite through
344           minimal aqueous alteration in a small porous icy body. *Geochimica et Cosmochimica*
345           *Acta* **214**, 172-190, doi:https://doi.org/10.1016/j.gca.2017.06.047 (2017).

346    35    Cody, G. D. *et al.* Quantitative organic and light-element analysis of comet 81P/Wild 2
347           particles using C-, N-, and O-μ-XANES. *Meteoritics & Planetary Science* **43**, 353-365
348           (2008).

349    36    Kissel, J. & Krueger, F. The organic component in dust from comet Halley as measured
350           by the PUMA mass spectrometer on board Vega 1. *Nature* **326**, 755-760 (1987).

351    37    Flynn, G. J., Keller, L. P., Feser, M., Wirick, S. & Jacobsen, C. The origin of organic
352           matter in the solar system: Evidence from the interplanetary dust particles. *Geochimica et*
353           *Cosmochimica Acta* **67**, 4791-4806, doi:10.1016/j.gca.2003.09.001 (2003).

354    38    Keller, L. P. *et al.* The nature of molecular cloud material in interplanetary dust.
355           *Geochimica et Cosmochimica Acta* **68**, 2577-2589, doi:10.1016/j.gca.2003.10.044 (2004).

356    39    Noguchi, T. *et al.* Variation of mineralogy and organic material during the early stages of
357          aqueous activity recorded in Antarctic micrometeorites. *Geochimica et Cosmochimica*
358          *Acta* **208**, 119-144, doi:10.1016/j.gca.2017.03.034 (2017).

359    40    Alleon, J., Bernard, S., Remusat, L. & Robert, F. Estimation of nitrogen-to-carbon ratios
360          of organics and carbon materials at the submicrometer scale. *Carbon* **84**, 290-298,
361          doi:10.1016/j.carbon.2014.11.044 (2015).

362    41    De Gregorio, B. T. *et al.* Isotopic and chemical variation of organic nanoglobules in
363          primitive meteorites. *Meteoritics & Planetary Science* **48**, 904-928,
364          doi:10.1111/maps.12109 (2013).

365    42    Yurimoto, H. *et al.* Isotopic compositions of asteroidal liquid water trapped in fluid
366          inclusions of chondrites. *Geochemical Journal* **48**, 549-560,
367          doi:10.2343/geochemj.2.0335 (2014).

368    43    Pizzarello, S. & Williams, L. B. Ammonia in the early Solar System: An account from
369          carbonaceous meteorites. *The Astrophysical Journal* **749**, 161, doi:10.1088/0004-
370          637x/749/2/161 (2012).

371    44    De Sanctis, M. C. *et al.* Bright carbonate deposits as evidence of aqueous alteration on
372          (1) Ceres. *Nature* **536**, 54-57, doi:10.1038/nature18290 (2016).

373    45    Postberg, F. *et al.* Sodium salts in E-ring ice grains from an ocean below the surface of
374          Enceladus. *Nature* **459**, 1098-1101,
375          doi:http://www.nature.com/nature/journal/v459/n7250/suppinfo/nature08046_S1.html
376          (2009).

377    46    Takeichi, Y., Inami, N., Suga, H., Ono, K. & Takahashi, Y. Development of a compact
378          scanning transmission X-ray microscope (STXM) at the photon factory. *Chemistry*
379          *Letters* **43**, 373-375 (2014).

380    47    Takeichi, Y. *et al.* Design and performance of a compact scanning transmission X-ray
381          microscope at the Photon Factory. *Review of Scientific Instruments* **87**, 013704 (2016).

382    48    Ito, M. & Messenger, S. Isotopic imaging of refractory inclusions in meteorites with the
383          NanoSIMS 50L. *Applied Surface Science* **255**, 1446-1450,
384          doi:10.1016/j.apsusc.2008.05.095 (2008).

385    49    Ito, M. *et al.* H, C, and N isotopic compositions of Hayabusa category 3 organic samples.
386          *Earth, Planets and Space* **66**, 91, doi:10.1186/1880-5981-66-91 (2014).
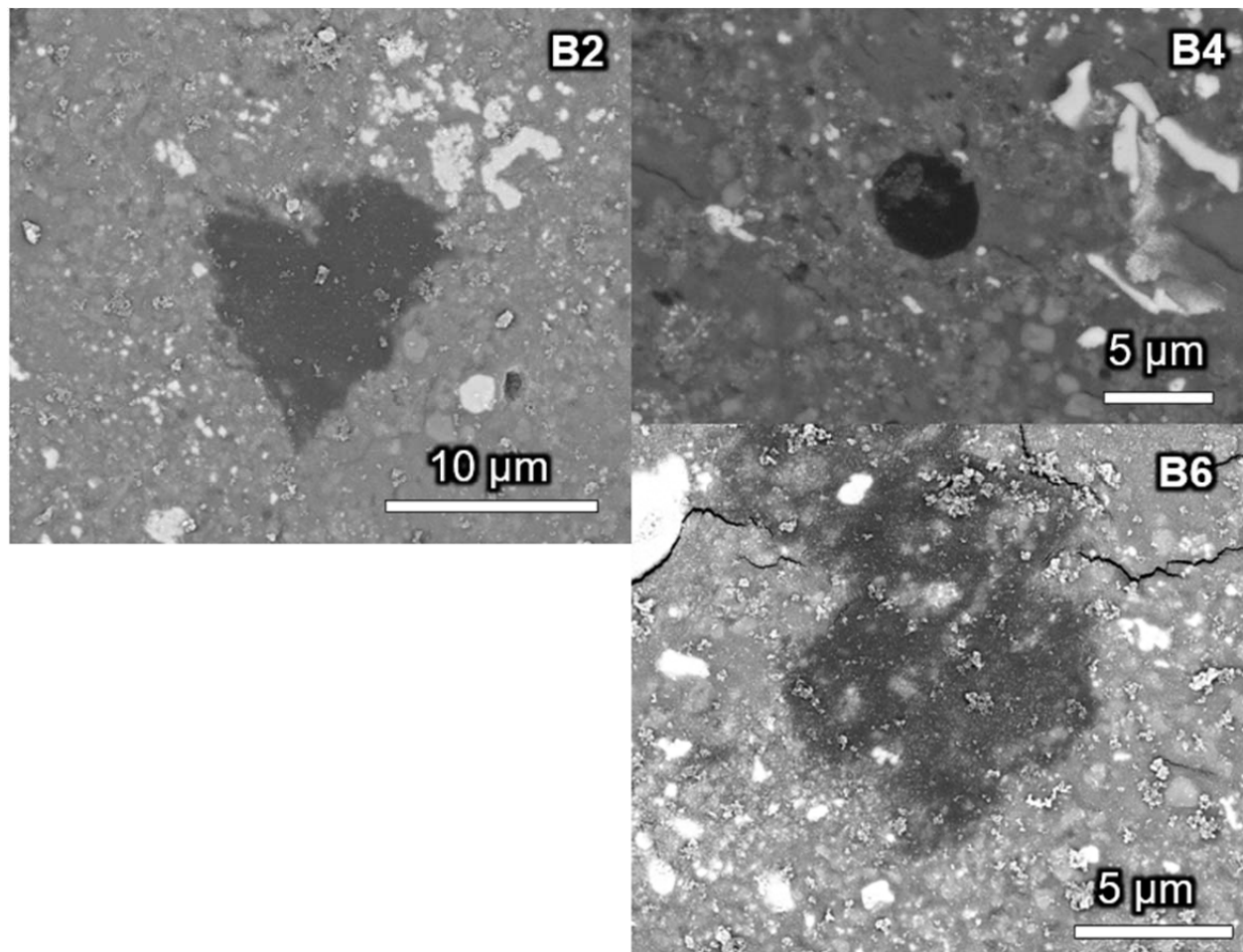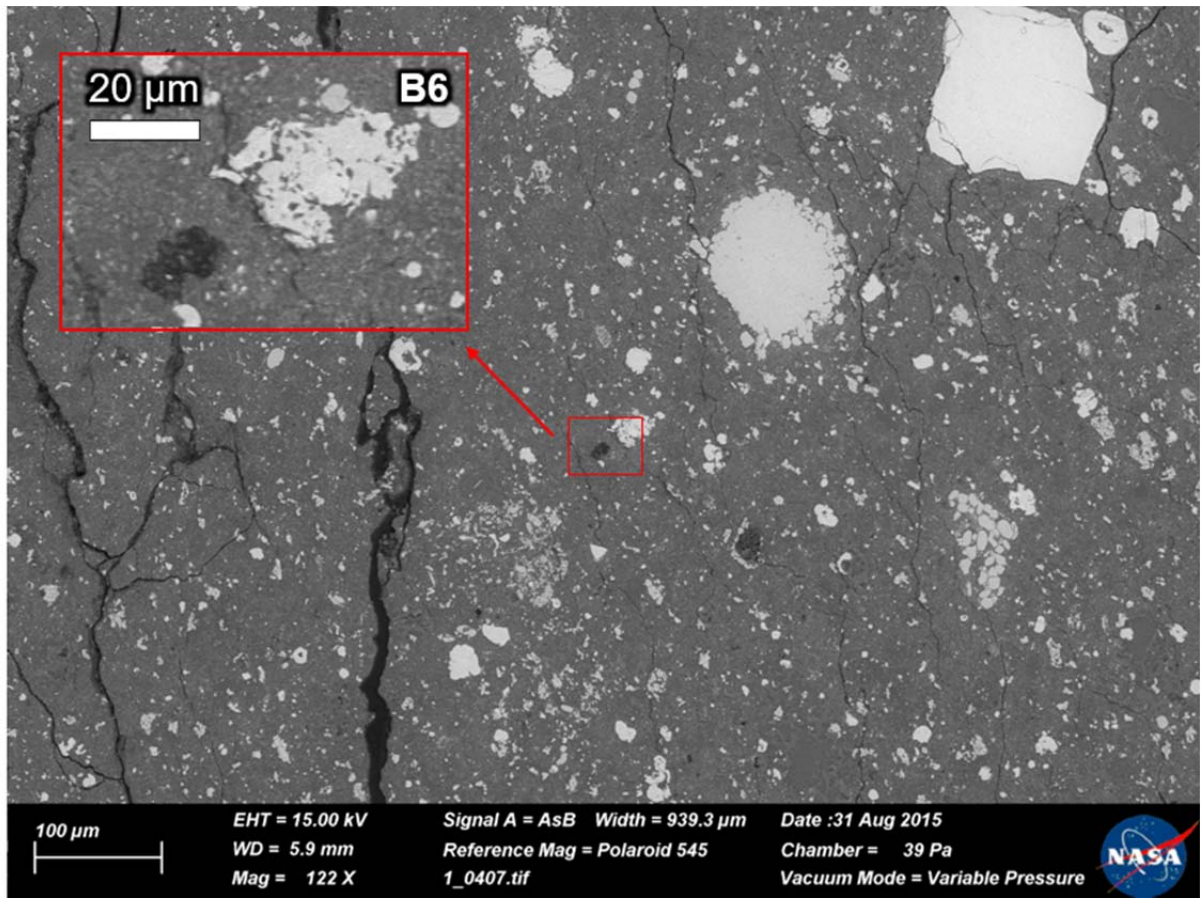
387

388

389

390

391

392

**Extended Data**
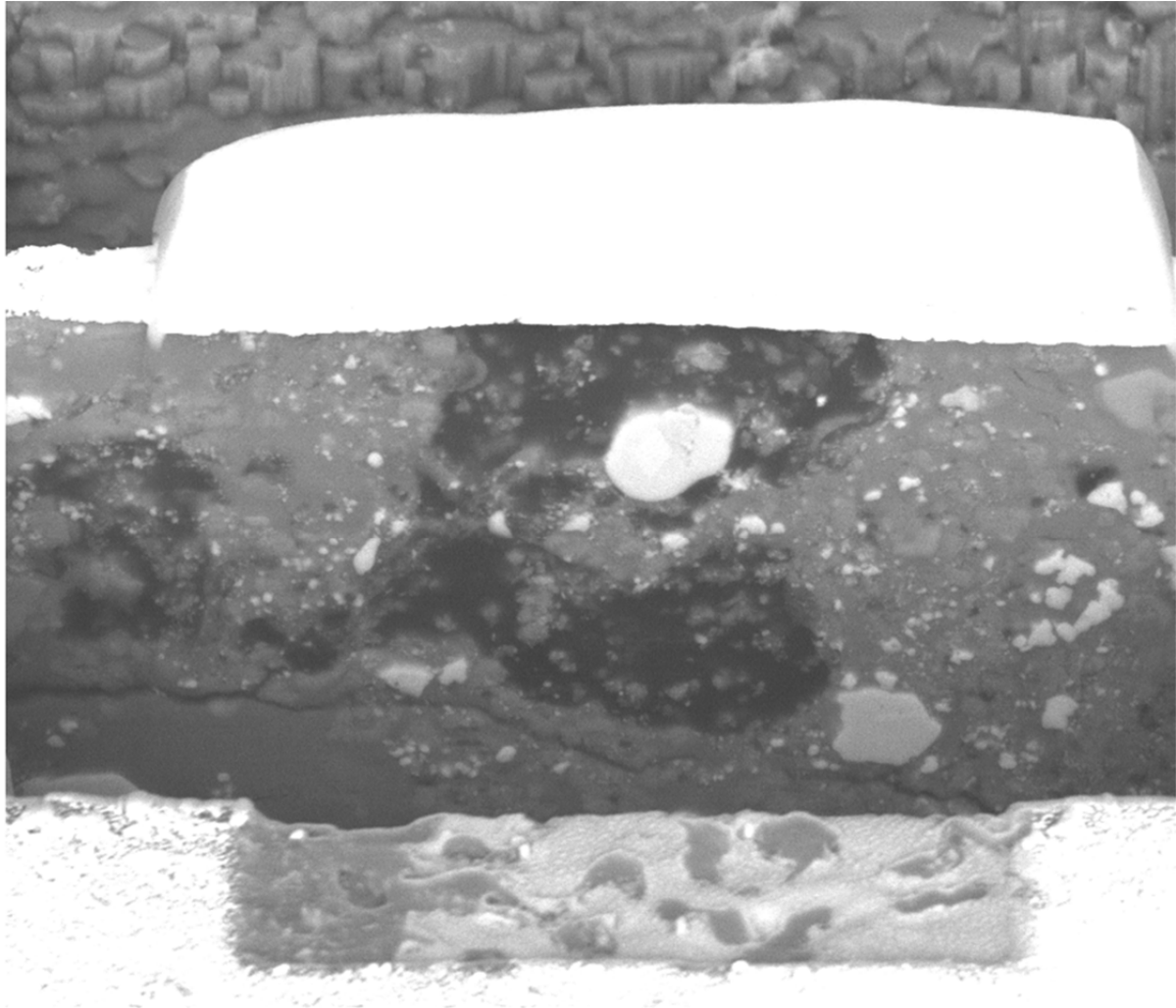
393

394



395

Extended Data Figure 1: **Backscattered electron images (BEI) of organic grains/aggregates (black) in the clast in the Zag clast.**

396
397

398

**a**

20 µm    B6

100 µm

EHT = 15.00 kV    Signal A = AsB    Width = 939.3 µm    Date :31 Aug 2015
WD = 5.9 mm     Reference Mag = Polaroid 545    Chamber =    39 Pa
Mag =    122 X    1_0407.tif    Vacuum Mode = Variable Pressure

399

**b**

HV: 10.0 kV | mag ⊞: 6 000 x | WD: 9.6 mm | tilt: 53 ° | mode: Z Cont | —— 10 µm —— NASA - JSC [Quanta 3D FEG]

400

401 Extended Data Figure 2: **Images of before and during sample preparation.** (a) Backscatter
402 electron image of the clast from the Zag meteorite. The OM aggregate analyzed here is shown in
403 red squares. (b) Backscatter electron image of the focused ion beam (FIB) section from the OM
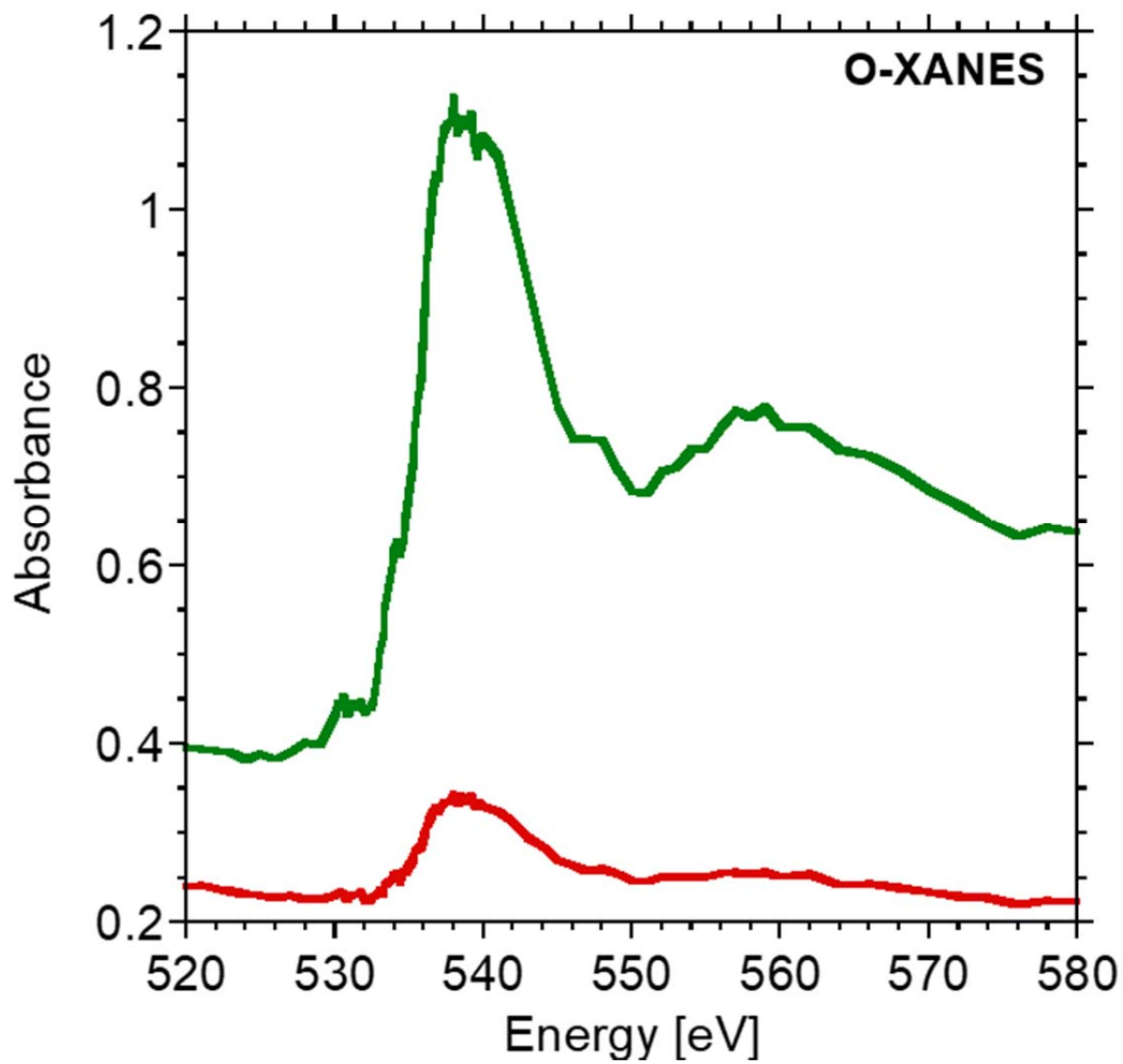404 aggregate in the Zag clast during the FIB milling process.

405
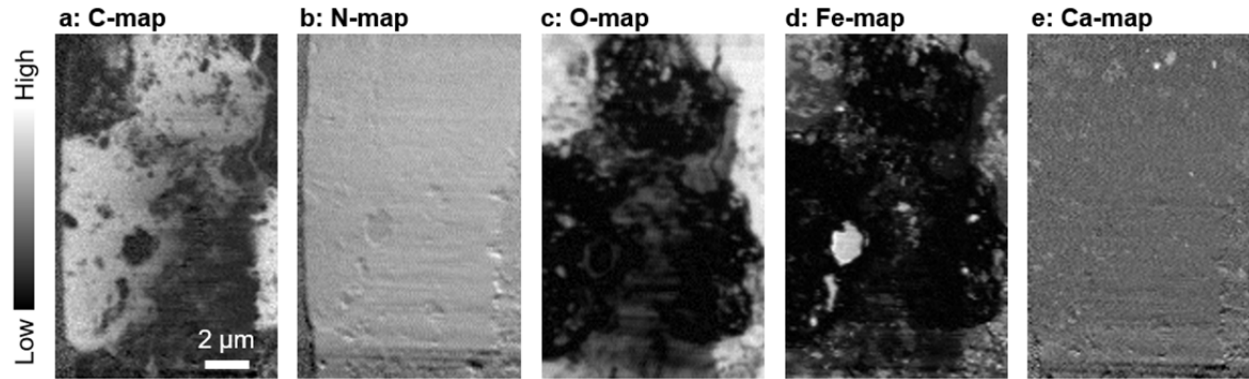
Extended Data Figure 3: **STXM elemental map of the FIB section including the OM aggregates in the Zag clast.** (a) C-map: $-\ln(I_{292}/I_{280})$, (b) N-map: $-\ln(I_{405}/I_{395})$, (c) O-map: $-\ln(I_{539}/I_{525})$, (d) Fe-map: $-\ln(I_{709}/I_{705})$, and (e) Ca-map: $-\ln(I_{349}/I_{345})$.

411

Extended Data Figure 4: **O-XANES spectra of the Zag clast.** The OM aggregate is shown in red, and surrounding matrix is in green.

412

413

414

415